

## Article

# Influence of Surface Methane on Tropospheric Ozone Concentrations and Cereal Yield in Asia

Kenichi Tatsumi 

School of Data Science, Nagoya City University, Nagoya 467-8501, Japan; tatsumi@ds.nagoya-cu.ac.jp

**Abstract:** Methane (CH<sub>4</sub>) emanating from terrestrial sources serves as a precursor for the genesis of tropospheric ozone (O<sub>3</sub>), a pernicious atmospheric contaminant that adversely modulates the physiological mechanisms of agricultural crops. Despite the acknowledged role of CH<sub>4</sub> in amplifying O<sub>3</sub> concentrations, the extant literature offers limited quantitative evaluations concerning the repercussions of CH<sub>4</sub>-mediated O<sub>3</sub> on cereal yields. Employing the GEOS-Chem atmospheric chemistry model, the present investigation elucidates the ramifications of a 50% diminution in anthropogenic CH<sub>4</sub> concentrations on the yield losses of maize, soybean, and wheat across Asia for the fiscal year 2010. The findings unveil pronounced yield detriments attributable to O<sub>3</sub>-induced phytotoxicity, with the Indo-Gangetic Plain and the North China Plain manifesting the most substantial yield impairments among the crops examined. A halving of anthropogenic CH<sub>4</sub> effluents could ameliorate considerable losses in cereal production across these agriculturally pivotal regions. CH<sub>4</sub>-facilitated O<sub>3</sub> exerts a pernicious influence on cereal yields; nevertheless, targeted mitigation of CH<sub>4</sub> effluents, particularly in the vicinity of the North China Plain, holds the potential to substantially attenuate O<sub>3</sub> contamination, thereby catalyzing an enhancement in regional cereal production.

**Keywords:** atmospheric chemistry model; AOT40; cereal; methane; ozone; production loss



**Citation:** Tatsumi, K. Influence of Surface Methane on Tropospheric Ozone Concentrations and Cereal Yield in Asia. *Agronomy* **2023**, *13*, 2586. <https://doi.org/10.3390/agronomy13102586>

Academic Editors: Julietta Moustaka and Michael Moustakas

Received: 28 September 2023

Revised: 3 October 2023

Accepted: 4 October 2023

Published: 9 October 2023



**Copyright:** © 2023 by the author. Licensee MDPI, Basel, Switzerland. This article is an open access article distributed under the terms and conditions of the Creative Commons Attribution (CC BY) license (<https://creativecommons.org/licenses/by/4.0/>).

## 1. Introduction

Methane (CH<sub>4</sub>) constitutes a volatile anthropogenic organic compound of considerable potency, serving as a salient precursor to tropospheric ozone (O<sub>3</sub>), nitrogen oxides (NO<sub>x</sub>), non-methane volatile organic compounds (NMVOCs), and carbon oxide (CO) [1]. When released into the atmosphere, CH<sub>4</sub> reacts with hydroxyl radicals (OH) to produce formaldehyde and other intermediate compounds. In the presence of nitrogen oxides (NO<sub>x</sub>) and sunlight, these intermediates undergo photochemical reactions, leading to the production of O<sub>3</sub> [2,3]. Furthermore, CH<sub>4</sub> functions as a potent, ephemeral climate pollutant, contributing to the genesis of ground-level O<sub>3</sub>, thereby detrimentally impacting human health and ecological systems [4]. The measurement of CH<sub>4</sub> is mainly conducted using gas chromatography, cavity ring-down spectroscopy, tunable diode laser absorption spectroscopy, and Fourier transform infrared spectroscopy, which allow for precise quantification of CH<sub>4</sub> concentrations in the atmosphere [5]. The primary sources of CH<sub>4</sub> can be broadly categorized into natural (40% of contemporary global CH<sub>4</sub> emissions) and anthropogenic origins (60% of contemporary global CH<sub>4</sub> emissions) [6]. Natural sources include wetlands, termites, oceans, freshwater bodies, and certain types of vegetation. Wetlands are the largest natural source, with microbial activity in anaerobic environments producing CH<sub>4</sub> as a byproduct. Anthropogenic sources, on the other hand, are a result of human activities and include agricultural activities such as enteric fermentation from ruminants, rice paddies, and manure management. The energy sector also contributes significantly to CH<sub>4</sub> emissions, especially from coal mining, oil and natural gas extraction, and transportation. Landfills are another major source, where organic waste decomposes anaerobically. Additionally, wastewater treatment processes and certain industrial processes also release CH<sub>4</sub>. Recent data from the National Oceanic and Atmospheric Administration (NOAA)

indicate an accelerated escalation in CH<sub>4</sub> concentrations over the past decade, culminating in an unprecedented growth rate in 2020 [7]. This upsurge is principally ascribed to burgeoning emissions emanating from sectors such as agriculture, fossil fuel extraction, landfill waste, and wastewater management [8]. Although the Global Methane Pledge, which launched at the COP26 Conference of the Parties to the United Nations Framework Convention on Climate Change, set a goal of reducing CH<sub>4</sub> emissions by thirty percent by 2030 compared to 2020, projections suggest that anthropogenic CH<sub>4</sub> emissions are poised to augment further, reaching an estimated annual output of 380 million tons by 2030—an 8% increment relative to 2020 levels [9]. Consequently, the mitigation of CH<sub>4</sub> emissions emerges as an imperative strategy to confer immediate and enduring benefits upon climate, human health, ecosystems, and agricultural productivity [10].

O<sub>3</sub> exerts a pronounced deleterious influence upon crop yields and quality [11]. Empirical investigations by Avnery et al. [12] and Mills et al. [13] have elucidated that annual global yield deficits attributable to O<sub>3</sub> exposure range from 2.2 to 5.5% for maize, 8.5 to 14% for soybean, and 3.9 to 15% for wheat. Data from 2010 indicate that CH<sub>4</sub> emissions engendered global yield losses amounting to 25 Mt (Megaton) for soybean, 6.5 Mt for maize, and 45 Mt for wheat [10]. Shindell and Smith [14] posited that a reduction of 134 Mt in CH<sub>4</sub> emissions could forestall yield deficits of 2.23 Mt for soybeans, 5.58 Mt for maize, and 7.46 Mt for wheat on a global scale. The aggregate production loss per 134 Mt of CH<sub>4</sub> emitted in India and China is quantified as 0.147 Mt and 1.554 Mt for maize, 0.077 Mt and 0.047 Mt for soybean, and 2.700 Mt and 1.324 Mt for wheat, respectively [5]. Thus, the attenuation of CH<sub>4</sub> emissions is pivotal in mitigating ground-level O<sub>3</sub> concentrations globally and in fostering sustainable agricultural production. Atmospheric chemical models that estimate CH<sub>4</sub> emissions and their concomitant impact on surface O<sub>3</sub> concentrations are instrumental in calibrating emissions, identifying efficacious mitigation strategies, and evaluating the repercussions of diminished surface CH<sub>4</sub> background concentrations on cereal yields. However, the extant literature offers limited insights into how reductions in CH<sub>4</sub> emissions could obviate grain yield deficits.

The present study undertakes an exhaustive exploration of the interrelationship between CH<sub>4</sub>-induced O<sub>3</sub> and cereal productivity (maize, soybean, and wheat) within the Asian continent. While extant modeling endeavors have predominantly focused on national trajectories, a paucity of studies have probed the correlation between O<sub>3</sub> responses to CH<sub>4</sub> emissions and cereal yields in Asia, utilizing atmospheric chemistry models to simulate sub-grid scale data. A salient feature of this investigation is its assessment of the nexus between O<sub>3</sub> and cereal yield and production under a scenario involving a 50% reduction in anthropogenic CH<sub>4</sub> emissions. The primary objectives of this study are: (1) to scrutinize O<sub>3</sub> exposure metrics via AOT40 (accumulated O<sub>3</sub> exposure surpassing a 40 ppb threshold), and (2) to quantitatively evaluate the yield and production deficits of cereals in Asia attributable to CH<sub>4</sub>-induced O<sub>3</sub> exposure.

## 2. Materials and Methods

### 2.1. Model Description

For the purposes of this investigation, the GEOS-Chem atmospheric chemistry model (version 13.3.4), as delineated by Bey et al. [15], was employed to scrutinize the ramifications on cereal yield and production consequent to a 50% diminution in anthropogenic CH<sub>4</sub> emissions, utilizing the year 2010 as the baseline reference (Table 1). The GEOS-Chem model was configured to operate within two distinct domains for nested grid simulation. Initially, a comprehensive global simulation incorporating a full-chemistry mechanism was executed to ascertain the lateral boundary conditions (BC) for a nested child domain, characterized by a 4° × 5° grid resolution and encompassing 72 vertical strata, with global coverage spanning the temporal interval from 1 January 1990 to 31 December 2010, Coordinated Universal Time (UTC). Subsequently, a high-resolution nested grid simulation was conducted, featuring a 0.5° × 0.625° horizontal resolution and 72 vertical layers extending from the Earth's surface to an altitude of 0.01 hPa. This simulation was

geographically confined to East, South, and Southeast Asia (11° S–55° N, 60° E–150° E) and temporally bounded between 1 January 2009 and 31 December 2010, UTC, utilizing the BC derived from the preceding global simulation. The selection of 2010 as the benchmark year was predicated on the accessibility of verifiable emission and cereal yield data extant up to that juncture. Temporal discretization was established with a time step of 300 s for transport and convective processes, and 600 s for chemical reactions and emissions. A spin-up duration of 20 years was allocated for the external domain, whereas a 1 year spin-up period was designated for the internal domain.

**Table 1.** Computational scenarios of methane emissions employed in the study.

Scenario	CH <sub>4</sub> Mixing Ratio (ppbv) or Emissions	Source
BASE	1808	[16]
HALF	50% anthropogenic CH <sub>4</sub> reduction	[2]

## 2.2. Emission and Meteorological Data

The Community Emissions Data System (CEDS v2021-06) served as the foundational repository for global monthly mean anthropogenic emissions, featuring a horizontal resolution of  $0.5^\circ \times 0.5^\circ$ . This comprehensive dataset encompasses an array of emissions, including CO, CO<sub>2</sub>, NO<sub>x</sub>, SO<sub>2</sub>, NH<sub>3</sub>, NMVOCs, and organic/black carbon, emanating from diverse sectors such as non-combustion agriculture, energy transformation and extraction, industrial combustion and processes, surface transportation, residential and commercial activities, solvents, waste management, and international maritime operations. Surface CH<sub>4</sub> mixing ratios were procured from WMO Greenhouse Gas Bulletin [16]. Emissions attributable to biomass burning were sourced from the Global Fire Emissions Dataset v4.1 (GFED4; [17]), while dust and sea salt emissions were derived from the pertinent literature [18,19]. Lightning-induced NO<sub>x</sub> emissions and soil-originated NO<sub>x</sub> emissions were obtained from designated references [20,21]. The Model of Emissions of Gases and Aerosols from Nature version 2.1 (MEGAN2.1) was employed to ascertain the monthly biogenic emissions inventory, which quantifies the net flux of isoprene, monoterpenes, and other trace gases and aerosols released into the atmosphere by ecological systems [22]. Meteorological initial boundary conditions were acquired from the Modern-Era Retrospective Analysis for Research and Applications version 2 (MERRA-2) dataset [23], a global atmospheric reanalysis orchestrated by NASA's Global Modeling and Assimilation Office (GMAO), characterized by a native  $0.5^\circ \times 0.625^\circ$  horizontal resolution and 72 hybrid sigma/pressure levels [24]. The intricate emission and meteorological datasets were procured and assimilated into the GEOS-Chem model through the Harmonized Emissions Component (HEMCO) (version 3.2.2), a sophisticated software module designed for calculating atmospheric emissions from diverse sources, regions, and species on a user-specified grid [25].

## 2.3. Observation Dataset

The cereal production datasets for the year 2010, employed in this investigation, were extracted from the Global Agro-Ecological Zones (GAEZ v4) repository [26]. The GAEZ dataset is formulated through the transformation of national production statistics into a gridded framework, utilizing a sophisticated downscaling methodology that amalgamates land attributes, geospatial intelligence (either empirically observed or inferentially deduced, such as remotely sensed land cover, pedological features, climatic conditions, and vegetative distribution), and population density metrics. This comprehensive dataset encapsulates spatially mapped distributions of harvested regions, yield indices, and production metrics at a resolution of 5 arc-minute grid cells. Subsequently, this information was meticulously tailored to conform to the grid dimensions of the GEOS-Chem model. Temporally specific data pertaining to cereal sowing and reaping timelines were acquired from the Crop Calendar Dataset [27] and were subsequently employed in the calculation of the AOT40 indices pertinent to the vegetative growth phase.

#### 2.4. Cereal Yield and Production Losses Based on Ozone Exposure Indices

The metrics predicated on O<sub>3</sub> exposure were ascertained for the inaugural trimester of the 2010 vegetative growth cycle [28]. It is noteworthy that the exposure-response function exhibits regional heterogeneity and is modulated by variations in statistical methodologies as well as divergent definitions of the growing season. Notwithstanding the considerable uncertainties concomitant with the utilization of exposure metrics for the prognostication of cereal yield detriments [29,30], this investigation leveraged the AOT40 index as an efficacious instrument for such estimations. AOT40 values, aggregating to 3 ppmh over a three-month cultivation interval, are congruent with the critical thresholds delineated for crop safeguarding, signifying a 5% yield decrement. This AOT40 index has been ubiquitously adopted by authoritative bodies such as the United Nations Economic Commission for Europe, the United States Environmental Protection Agency (USEPA), and the World Meteorological Organization (WMO) for the evaluation of phytotoxic risks associated with O<sub>3</sub> exposure, as well as for the quantification of agronomic yield and production deficits attributable to surface O<sub>3</sub> exposure across disparate geographies [6,31]. The computational methodology for the AOT40 indices was executed in accordance with Equation (1), elaborated hereinbelow:

$$\text{AOT40} = \sum_{i=1}^n ([\text{O}_3]_i - 0.04), \text{ for } \text{O}_3 \geq 0.04 \text{ ppmv from } 8:00 \text{ to } 19:59 \text{ (LST)}, \quad (1)$$

wherein  $[\text{O}_3]_i$  represents the hourly mean surface O<sub>3</sub> concentration expressed in ppmv, and  $n$  denotes the aggregate number of hours encompassing the three-month vegetative growth phase.

The deduced relative yield (RY) of the cereal crop was subtracted from unity to ascertain the O<sub>3</sub>-induced relative yield loss (RYL) in accordance with the subsequent equation:

$$\text{RYL} = 1.0 - \text{RY}, \quad (2)$$

wherein RY constitutes the relative grain yield, factoring in the deleterious effects of O<sub>3</sub> exposure. Conversely, RYL represents the decrement in grain yield relative to the theoretical yield devoid of O<sub>3</sub>-induced impairments. The estimation of RY was predicated upon the empirical correlation delineated for the AOT40 index [32], as elucidated in the subsequent equation:

$$\text{RY} = -0.0036 \times \text{AOT40} + 1.02 \quad \text{for maize}, \quad (3)$$

$$\text{RY} = -0.0116 \times \text{AOT40} + 1.02 \quad \text{for soybean}, \quad (4)$$

$$\text{RY} = -0.0161 \times \text{AOT40} + 0.99 \quad \text{for wheat} \quad (5)$$

The quantification of crop production loss (CPL) was executed employing Equation (6), applied to each individual grid cell  $i$  within the grain cultivation zone. This calculation utilized the RYL metric in conjunction with the empirically verified rice production data for the year 2010, as procured from the Global Agro-Ecological Zones (GAEZ) repository.

$$\text{CPL}_i = \text{CP}_i \times \text{RYL}_i / (1 - \text{RYL}_i) \quad (6)$$

wherein CP denotes the empirically verified grain production, as sourced from the Global Agro-Ecological Zones (GAEZ) database.

### 3. Results and Discussion

#### 3.1. Methane and Ozone Spatial Distributions

The CH<sub>4</sub> mixing ratio in China, Korea, and Japan exhibited a pronounced elevation compared to other nations, a phenomenon predominantly influenced by CH<sub>4</sub> emanations originating from the North China Plain (Figure S1). This elevated ratio is reflective of anthropogenic CH<sub>4</sub> discharges from diverse sources, including coal combustion, natural

gas extraction, and landfill operations, particularly in the Beijing-Tianjin-Hebei (BTH) region [33]. The advective transport of this augmented CH<sub>4</sub> mixing ratio from the BTH region to Korea and Japan can elucidate the intensified CH<sub>4</sub> concentrations observed during the summer months, as well as the elevated baseline levels in China, Korea, and Japan. Zonal mean analyses of surface CH<sub>4</sub> between latitudes 30 and 40° N disclosed that CH<sub>4</sub> concentrations within the lower troposphere over the North China Plain remained consistently elevated throughout the annual cycle (Figure S2).

Surface O<sub>3</sub> mixing ratios reached their zenith from winter to spring across all nations, with the exception of China, Korea, Japan, and Pakistan (Figure 1). Nevertheless, the summer O<sub>3</sub> baseline in these four countries was comparatively elevated. The winter and spring amplification of O<sub>3</sub> concentrations in most nations, excluding the aforementioned quartet, can be ascribed to the photolytic disintegration of O<sub>3</sub>, succeeded by the reaction of O(<sup>1</sup>D) atoms with copious water vapor during the summer, as well as the reaction of hydroxyl radicals with O<sub>3</sub>, culminating in O<sub>3</sub> depletion. Additionally, the incursion of pristine oceanic air masses, facilitated by the Asian summer monsoon, serves to attenuate O<sub>3</sub> concentrations during the summer months in relatively lower latitude zones. In contrast, the summer apogee in O<sub>3</sub> mixing ratios in China, Japan, and Korea is principally attributable to (1) the northward advective transport of O<sub>3</sub> engendered by the Asian summer monsoon, and (2) the augmented CH<sub>4</sub> discharges in the BTH region (Figure 1). Elevated summer O<sub>3</sub> concentrations in Pakistan may be ascribed to the impediment of the summer southwest monsoon by topographical barriers such as the Karakoram range, Hindu Kush mountains, and the Himalayas, resulting in the entrapment of elevated O<sub>3</sub> concentrations. These O<sub>3</sub> trends are congruent with extant findings [34]. Ultimately, while meteorological and topographical factors exert influence, CH<sub>4</sub> discharges from key sectors, including coal, agriculture, and petroleum, emerge as salient contributors to O<sub>3</sub> concentrations in the North China Plain. Consequently, the mitigation of CH<sub>4</sub> emissions in the North China Plain could engender a concomitant reduction in AOT40 values within this region.

### 3.2. Spatial Distributions of Surface Accumulated Ozone Exposure Metrics

Augmented summertime surface O<sub>3</sub> concentrations are discernible in both the Indo-Gangetic Plain and the North China Plain, regions that serve as pivotal granary zones in India and China, respectively. These locales are concurrently subjected to the most acute O<sub>3</sub> contamination (Figure 1). The profusion of O<sub>3</sub> precursor emissions in these vicinities catalyzes O<sub>3</sub> genesis and accrual, modulated by variables such as advective wind patterns, elevated barometric pressure, and atmospheric pollutant recirculation. Figure 2 delineates the spatial distribution of AOT40 metrics for maize, soybean, spring wheat, and winter wheat under the BASE and HALF simulation paradigm. The mean AOT40 values for maize, soybean, spring wheat, and winter wheat in cultivated regions under the BASE simulation were 17.9 ppmh, 17.5 ppmh, 17.5 ppmh, and 6.7 ppmh, respectively. The decremental rates of AOT40 under the HALF simulation were 18% for maize, 19% for soybean, 19% for spring wheat, and 23% for winter wheat, respectively (Tables 2 and 3).

Mitigating CH<sub>4</sub> emissions could forestall the exacerbation of O<sub>3</sub> contamination episodes during the cereal cultivation season. The majority of regions surpassed the UNECE and WHO stipulated critical thresholds based on AOT40 metrics (3 ppmh for a trimester), which are concomitant with a 5% diminution in the yield of pivotal cereal crops in Asia. Noteworthy AOT40 epicenters were discerned in the Indo-Gangetic and North China Plains. Conversely, the southern territories of India manifested comparatively attenuated AOT40 indices for all cereals, while Southeast Asia exhibited diminished values specifically for maize and soybean. In India, studies by Deb Roy et al. [35] and Tai et al. [36] underscored that AOT40 metrics in the fecund Indo-Gangetic Plain persistently exceeded those in other Indian locales, corroborated by both observational and computational analyses. The simulated AOT40 indices in this investigation were conspicuously elevated over the Indo-Gangetic Plain, portending potential deleterious impacts on agrarian yields. This amplification is ascribable to the region's abundance of O<sub>3</sub> precursors, engendered by

significant anthropogenic endeavors, including coal-fired thermoelectric power generation and the extraction of ferrous and fossil fuels [37,38].

Furthermore, the area's barometric configurations, aerodynamic orientations, velocities, and topographical attributes are conducive to the photochemical accretion of  $O_3$ . In contrast, numerous sectors of central and southern India registered diminished AOT40 metrics, attributable to the incursion of pristine maritime air masses propelled by prevailing southwesterly airstreams [39]. Studies by Feng et al. [40] and Tai et al. [41] corroborated that the North China Plain exhibited relatively elevated AOT40 indices compared to central and southern China. The North China Plain is densely populated and vulnerable to anthropogenic effluents, predominantly emanating from fuel combustion. This locale is also characterized by unrelenting high-pressure systems, acute solar irradiance, low relative humidity, and moderate wind velocities, culminating in escalating  $O_3$  concentrations [41–43]. While direct juxtapositions are intricate owing to disparities in computational models and temporal scopes, the trends discerned in this study are congruent with antecedent scholarly investigations. One plausible explanation for the relatively subdued AOT40 levels in Asia's equatorial latitudes could be the incursion of air masses with attenuated  $O_3$  concentrations, a consequence of the southwest summer monsoon.

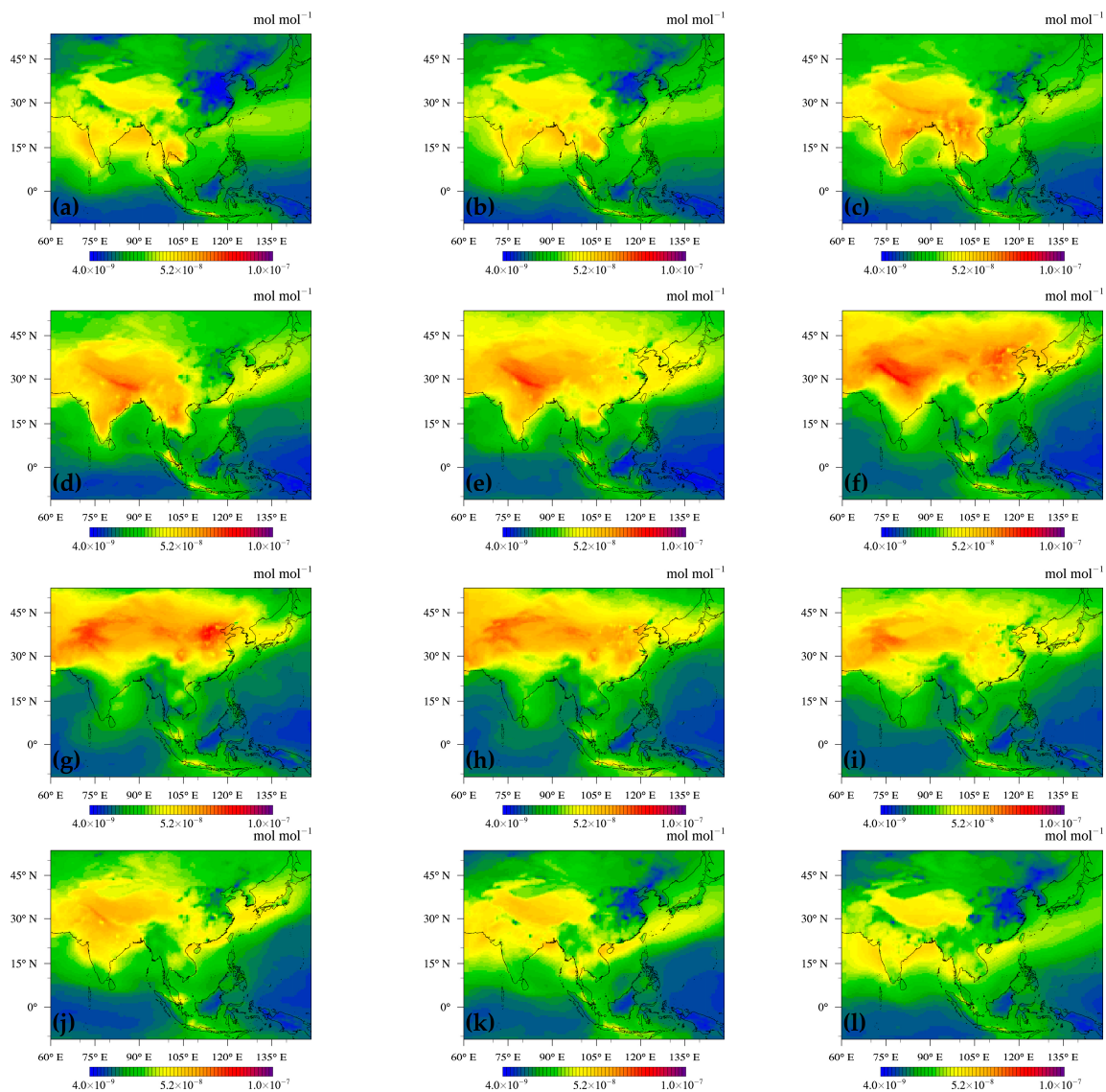


**Figure 1.** Surface  $O_3$  mixing ratio for 2010 at (a) January, (b) February, (c) March, (d) April, (e) May, (f) June, (g) July, (h) August, (i) September, (j) October, (k) November, and (l) December.

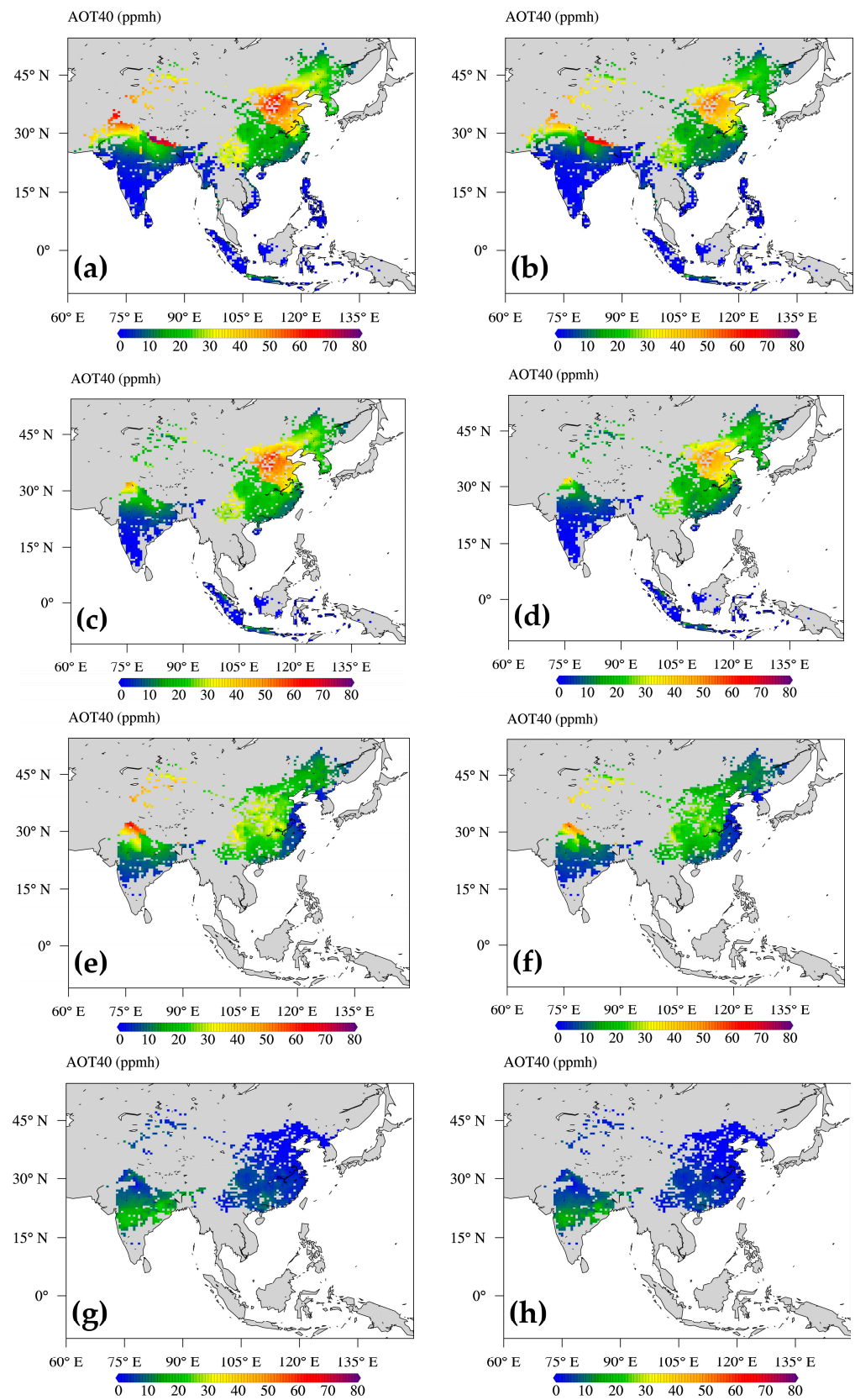


**Figure 2.** Spatial Distribution of surface-level AOT40 values for 2010 under BASE (left half) and HALF (right half) simulation. (a,b) Maize, (c,d) soybean, (e,f) spring wheat, (g,h) winter wheat.

**Table 2.** AOT40 (ppmh), relative yield losses (RYL; %), total crop production losses (CPL; Kt (Kiloton)) for maize and soybean across Asia countries for the year 2010 under BASE and HALF scenarios.

Country	BASE			HALF			BASE			HALF		
	Maize						Soybean					
	AOT40	RYL	CPL	AOT40	RYL	CPL	AOT40	RYL	CPL	AOT40	RYL	CPL
Republic of Korea	20.5	5.3	3.6	16.7	3.9	2.6	18.8	19.8	17.2	15.1	15.6	12.8
North Korea	22.2	6.1	87.8	18.1	4.6	65.5	21.9	23.4	59.1	17.9	18.8	44.8
China	26.7	7.4	14,616.2	22.5	5.9	11,685.5	25.2	26.5	3353.4	21.2	22.5	2761.7
Philippines	0.2	0.0	0.0	0.1	0.0	0.0	-	-	-	-	-	-
Vietnam	8.7	2.1	59.5	7.5	1.7	43.8	17.2	0.0	0.0	15.2	0.0	0.0
Cambodia	0.1	0.0	0.0	0.0	0.0	0.0	-	-	-	-	-	-
Laos	28.9	0.0	0.0	26.8	0.0	0.0	-	-	-	-	-	-
Thailand	6.3	0.9	0.0	5.3	0.6	0.0	-	-	-	-	-	-
Myanmar	3.7	0.3	2.0	3.0	0.2	1.7	13.3	8.8	0.0	11.5	7.8	0.0
Malaysia	0.0	0.0	0.0	0.0	0.0	0.0	-	-	-	-	-	-
Indonesia	1.4	0.2	30.0	1.1	0.1	16.0	2.4	2.1	5.5	1.9	1.6	3.8
Bangladesh	3.1	0.1	0.7	1.6	0.0	0.0	5.1	0.0	0.0	2.7	0.0	0.0
Nepal	65.3	21.3	484.0	57.6	18.5	404.3	15.9	13.9	0.0	10.8	8.1	0.0
Bhutan	36.6	8.7	0.0	30.5	7.2	0.0	5.4	4.3	0.0	2.7	1.1	0.0
India	9.2	2.0	284.6	6.4	1.2	182.1	8.3	7.8	128.5	5.5	4.8	62.9
Pakistan	32.9	10.1	608.8	25.6	7.5	450.0	37.3	34.9	0.0	29.8	29.1	0.0
Taiwan	7.9	0.9	0.3	5.6	0.2	0.1	-	-	-	-	-	-
Sri Lanka	0.6	0.0	0.0	0.3	0.0	0.0	-	-	-	-	-	-
Asia	17.9	4.7	16,177.4	14.6	3.6	12,851.7	17.5	18.2	3563.8	14.3	14.8	2865.4

**Table 3.** Same as Table 2 except spring and winter wheat.

Country	BASE			HALF			BASE			HALF		
	Spring Wheat						Winter Wheat					
	AOT40	RYL	CPL	AOT40	RYL	CPL	AOT40	RYL	CPL	AOT40	RYL	CPL
Republic of Korea	2.0	0.0	0.0	1.3	0.0	0.0	-	-	-	-	-	-
North Korea	3.4	6.5	7.6	2.3	4.8	5.5	0.2	1.4	1.5	0.1	1.2	1.3
China	18.9	31.0	54,774.3	15.8	26.3	42,455.6	3.9	7.3	4715.0	3.0	5.8	3639.9
Myanmar	15.5	26.1	0.5	12.9	21.9	0.4	2.2	4.6	0.1	1.9	4.0	0.0
Bangladesh	7.1	12.4	7.0	4.8	8.8	4.7	12.8	21.5	8.9	10.6	18.0	7.0
Nepal	15.1	24.5	108.3	10.6	17.6	71.4	9.8	16.8	64.0	7.8	13.5	49.4
Bhutan	29.4	31.4	0.1	24.4	29.2	0.1	10.5	17.9	0.1	8.6	14.8	0.0
India	15.5	23.2	40,465.4	11.5	18.2	30,927.6	12.0	20.3	10,862.2	9.4	16.1	7976.7
Pakistan	43.5	47.9	436.0	34.1	43.8	377.1	5.0	9.1	40.5	3.6	6.7	29.5
Asia	17.5	28.1	95,799.2	14.2	23.4	73,842.3	6.7	11.9	15,692.3	5.2	9.4	11,704.0

### 3.3. Ozone-Induced Relative Yield Losses and Consequent Production Deficits

Figure 3 elucidates the O<sub>3</sub>-mediated relative yield loss (RYL) for maize, soybean, spring wheat, and winter wheat under both BASE and HALF simulation scenarios. The spatial delineation of RYL, as gauged by AOT40 metrics, concurs with empirical evidence presented in prior studies [28,44]. As per the extant findings, all agronomically significant regions manifested discernible degrees of phytotoxic impairment and concomitant yield diminution. The consolidated mean RYLs predicated on AOT40 for the BASE simulation were 7.4% and 4.7% for maize, 26.5% and 18.2% for soybean, 30.9% and 28.1% for spring wheat, and 7.3% and 11.9% for winter wheat in China and East Asia, respectively (Tables 2 and 3). These estimations not only supersede the antecedent modeling values of 3.8% and 4.7% for maize, 11.4% and 20.9% for soybean, and 16.3% and 19.0% for wheat, as delineated by [45], but also eclipse the previously reported figures of

2–3% for maize, 7–8% for soybean, and 12–13% for wheat in East Asia, as documented by [28]. Nonetheless, these findings are largely congruent with the values delineated for maize (8.6%) and wheat (32.8%) in China, as elucidated by [40]. The highest RYL for maize, soybean, spring wheat, and winter wheat was discerned in Nepal (21.3%), Pakistan (34.9%), Pakistan (47.9%), and Bangladesh (21.5%), respectively.

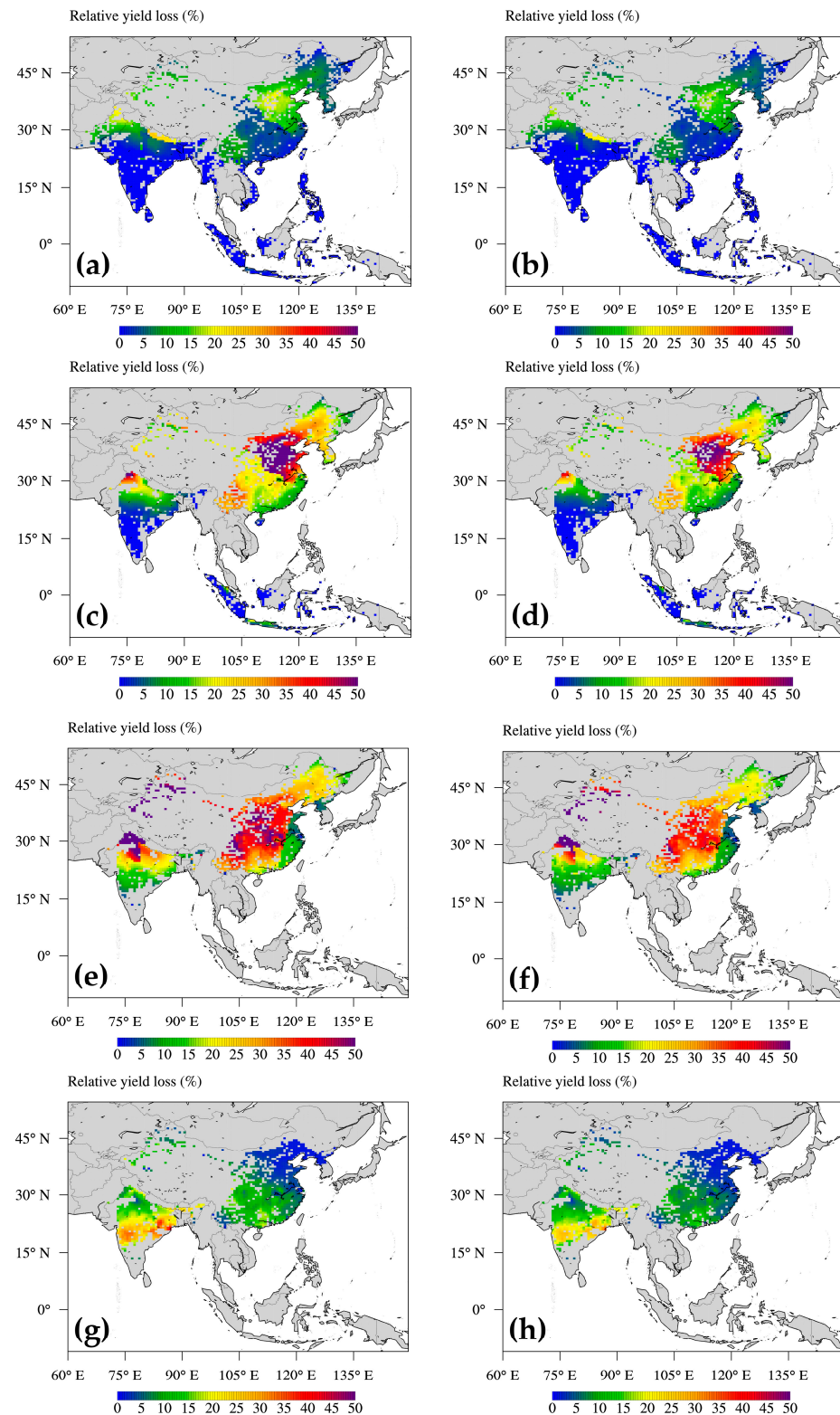


**Figure 3.** Relative yield loss (RYL) for 2010 under BASE (left) and HALF (right) scenarios. (a,b) Maize, (c,d) soybean, (e,f) spring wheat, and (g,h) winter wheat.

A discernible latitudinal gradient in relative yield loss (RYL) for maize, soybean, and spring wheat was manifest across East and South Asia (Figure 4). With the exception of winter wheat in the BASE scenario, the most pronounced O<sub>3</sub>-mediated RYL was localized in the industrially affluent and densely populated North China Plain, as well as the southern Himalayan region, which is subject to the influence of obstructed southern monsoon currents. Agronomic zones, barring winter wheat within the latitudinal band of 10 S–25 E, exhibited RYL values predicated on AOT40 metrics ranging from 0 to 10% for maize and soybean, and 5–15% for wheat. The decremental rates of RYL for the HALF scenario relative to the BASE were as follows: 23.1% for maize; 18.8% for soybean; 16.8% for spring wheat; and 20.9% for winter wheat (Figure 3 and Tables 2 and 3).

The regions exhibiting the most substantial crop production loss (CPL) for maize and soybean were localized in the North China Plain, whereas for spring wheat and winter wheat, these were concentrated in both the Indo-Gangetic Plain and the North China Plain—regions that also manifested elevated RYL metrics (Figure 4). The maximal aggregated CPL under the BASE scenario was observed in China for maize and soybean (14,616 Kt and 3353 Kt), and in India for spring wheat and winter wheat (40,465 Kt and 10,862 Kt) (Tables 2 and 3). The CPL decremental rates for the HALF scenario relative to the BASE were as follows: 3326 Kt for maize; 698 Kt for soybean; 21,957 Kt for spring wheat; and 3988 Kt for winter wheat (Figure 4 and Tables 2 and 3).

Shindell et al. [14] documented that the CPL resulting from a 50% decrease in anthropogenic CH<sub>4</sub> emissions in China and India amounted to 1554 Kt and 147 Kt for maize, and 47 Kt and 77 Kt for soybean, respectively. While the data sources and calculation conditions differ, leading to a broad range of uncertainties, a comparison with this research indicates that my results for maize and soybean were overestimated for China and underestimated for India (Table 2). These findings suggest that nullifying surface CH<sub>4</sub> background concentrations could mitigate production losses by approximately 1.4% for maize, 2.3% for soybean, and 13.0% for wheat across Asia's aggregate output. In summation, this inquiry lucidly delineates the characteristics of crop production deficits, particularly in the North China Plain and Indo-Gangetic Plain, regions characterized by elevated CH<sub>4</sub> concentrations. Such observations accentuate the imperative for nuanced investigations into the ramifications of CH<sub>4</sub> emissions on agronomic yield and productivity, particularly in the milieu of escalating surface O<sub>3</sub> concentrations across Asia.

### 3.4. Uncertainty Arising from Methane Emission Impacts

O<sub>3</sub> is synthesized through the photolytic interactions involving NO<sub>x</sub>, CO, NMVOCs, and CH<sub>4</sub> emissions. A fraction of tropospheric O<sub>3</sub> is advected from the stratosphere. Nonetheless, there exists a substantial ambiguity—approximately 50%—in the O<sub>3</sub> alterations attributable to CH<sub>4</sub> over the past four decades, as elucidated by multi-model assessments. These models incorporate the intricate interplay with NO<sub>x</sub>, the degradation chemistry of NMVOCs, and ensuing radical concentrations [46]. Approximately 55% of the O<sub>3</sub> budget augmentation since the pre-industrial epoch is ascribable to NO<sub>x</sub>, 25% to CH<sub>4</sub>, and 19% to CO and NMVOCs [47]. While computational studies underscore the salient contribution of CH<sub>4</sub> to O<sub>3</sub> genesis, the veracity of these models in prognosticating O<sub>3</sub> trajectories remains a subject of ongoing scrutiny (e.g., [48,49]). As a result, indeterminacies endure regarding the extent to which O<sub>3</sub> fluctuations can be correlated with ambient CH<sub>4</sub> concentrations.

Despite the inherent uncertainties, this study provides invaluable insights for regulatory stakeholders, aiding in the development and implementation of emission reduction strategies targeting O<sub>3</sub> precursors to enhance the predictability of future agricultural yields. Factors such as meteorological and soil conditions directly impact crop development. To further this research, it is essential to refine the input parameters of the GEOS-Chem atmospheric chemistry model using updated observational data, which will improve the precision of the simulations. Sensitivity analyses will be instrumental in quantifying the effects of individual parameters, highlighting areas for further refinement. Collaborative

efforts with field experts, coupled with advanced modeling techniques, will be pivotal in mitigating uncertainties. Additionally, by expanding the dataset to include more recent data and a wider array of sources, the robustness of the findings will be enhanced, offering a comprehensive understanding of the interplay between CH<sub>4</sub> emissions and O<sub>3</sub> concentrations. This holistic approach will allow for a more detailed evaluation of the combined effects of CH<sub>4</sub> and O<sub>3</sub> concentrations, meteorological factors, and climate changes on localized agricultural productivity.

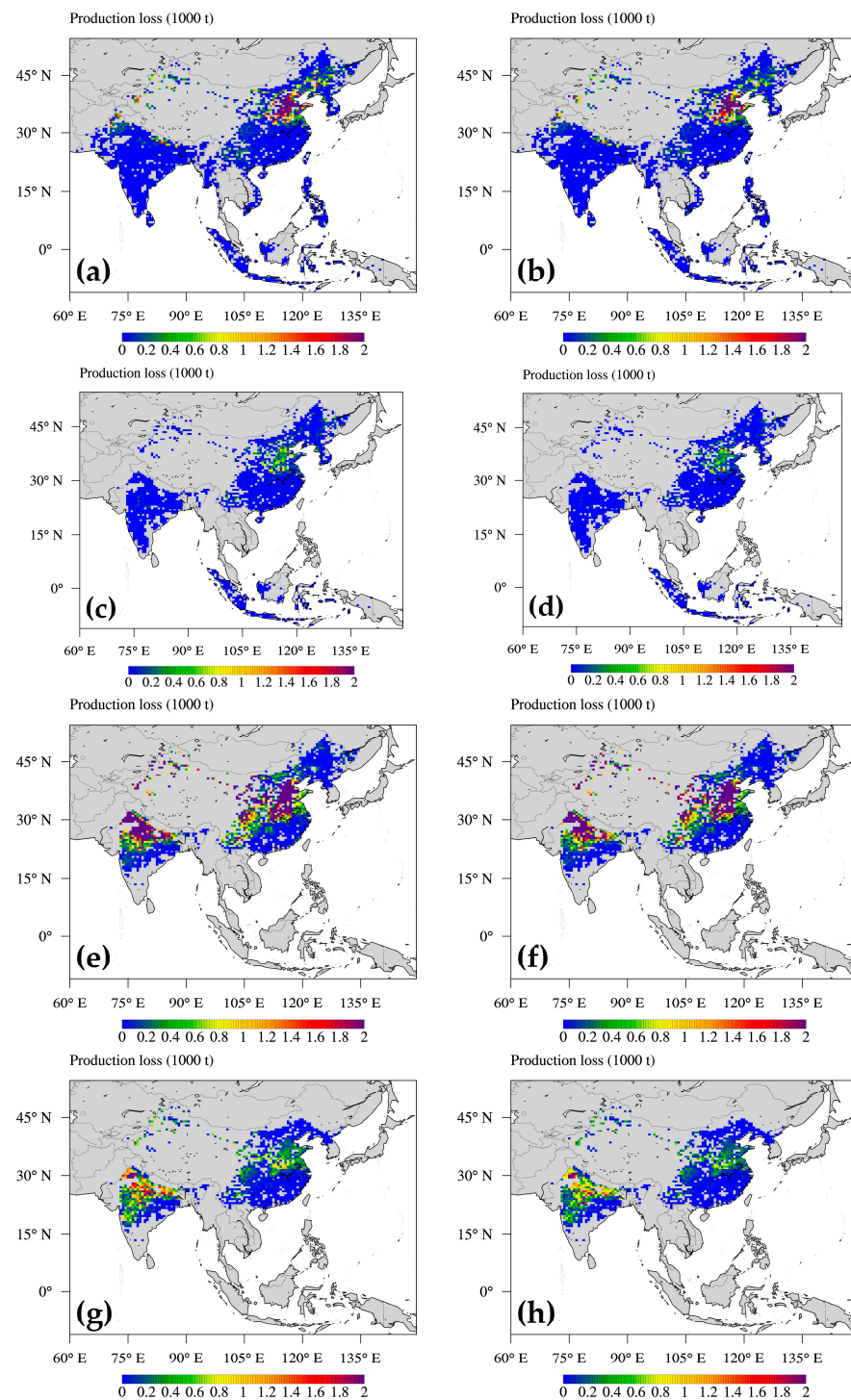


**Figure 4.** Crop production loss (CPL) for 2010 under BASE (left) and HALF (right) scenarios. (a,b) Maize, (c,d) soybean, (e,f) spring wheat, and (g,h) winter wheat.

#### 4. Conclusions

The mean O<sub>3</sub>-induced RYL for the BASE simulation across Asia was quantified as 4.7% for maize, 18.2% for soybean, 28.1% for spring wheat, and 11.9% for winter wheat. Moreover, the O<sub>3</sub>-induced detriments, as quantified by AOT40, approximated 16,177 Kt for maize, 3565 Kt for soybean, 95,799 Kt for spring wheat, and 15,692 Kt for winter wheat. Both RYL and CPL metrics were conspicuously elevated in the Indo-Gangetic Plain and the North China Plain relative to other Asian locales. Computational analyses elucidated that the abatement of CH<sub>4</sub> emissions could mitigate O<sub>3</sub>-induced impairments to maize, soybean, and wheat yields. A 50% decrement in anthropogenic CH<sub>4</sub> culminated in attenuations of cereal production losses in Asia, amounting to 3326 Kt for maize, 698 Kt for soybean, 21,957 Kt for spring wheat, and 3988 Kt for winter wheat, respectively.

Furthermore, the regulation of CH<sub>4</sub> emissions in the North China Plain could ameliorate O<sub>3</sub> contamination adversely affecting cereal yields in high-latitude regions, thereby accentuating the imperative of CH<sub>4</sub> emission curtailment. The gleaned insights from this investigation are envisaged to contribute to the formulation of a more efficacious and environmentally sustainable strategy to augment cereal productivity in the context of CH<sub>4</sub>-mediated O<sub>3</sub>.

**Supplementary Materials:** The following supporting information can be downloaded at: <https://www.mdpi.com/article/10.3390/agronomy13102586/s1>, Figure S1: Surface CH<sub>4</sub> mixing ratio for 2010 at (a) January, (b) February, (c) March, (d) April, (e) May, (f) June, (g) July, (h) August, (i) September, (j) October, (k) November, and (l) December.; Figure S2: Vertical structure of zonal (30–40° N) CH<sub>4</sub> for 2010 at (a) January, (b) February, (c) March, (d) April, (e) May, (f) June, (g) July, (h) August, (i) September, (j) October, (k) November, and (l) December.

**Funding:** This research was funded by JST PRESTO, grant number JPMJPR16O3 and JSPS KA-KENHI, grant number 16KK0169 and 19K15944.

**Data Availability Statement:** Data can be available upon the request of any scientist.

**Conflicts of Interest:** The author declares no conflict of interest.

#### References

1. West, J.J.; Fiore, A.M.; Horowitz, L.W.; Mauzerall, D.L. Global health benefits of mitigating ozone pollution with methane emission controls. *Proc. Natl. Acad. Sci. USA* **2006**, *103*, 3988–3993. [[CrossRef](#)] [[PubMed](#)]
2. Fiore, A.M.; Jacob, D.J.; Field, B.D.; Streets, D.G.; Fernandes, S.D.; Jang, C. Linking ozone pollution and climate change: The case for controlling methane. *Geophys. Res. Lett.* **2002**, *29*, 25-1–25-4. [[CrossRef](#)]
3. Holmes, C.D.; Prather, M.J.; Søvdø, O.A.; Myhre, G. Future methane, hydroxyl, and their uncertainties: Key climate and emission parameters for future predictions. *Atmos. Chem. Phys.* **2013**, *13*, 285–302. [[CrossRef](#)]
4. UNEP. Global Methane Assessment: Benefits and Costs of Mitigating Methane Emissions. Available online: <https://www.unep.org/resources/report/global-methane-assessment-benefits-and-costs-mitigating-methane-emissions> (accessed on 22 June 2022).
5. Dlugokencky, E.J.; Nisbet, E.G.; Fisher, R.; Lowry, D. Global atmospheric methane: Budget, changes and dangers. *Phil. Trans. R. Soc. A* **2011**, *369*, 2058–2072. [[CrossRef](#)] [[PubMed](#)]
6. Van Dingenen, R.; Dentener, F.J.; Raes, F.; Krol, M.C.; Emberson, L.; Cofala, J. The global impact of ozone on agricultural crop yields under current and future air quality legislation. *Atmos. Environ.* **2009**, *43*, 604–618. [[CrossRef](#)]
7. Thoning, K.; Dlugokencky, E.; Lan, X.; NOAA Global Monitoring Laboratory. Trends in Globally-Averaged CH<sub>4</sub>, N<sub>2</sub>O, and SF<sub>6</sub>. 2022. Available online: [https://gml.noaa.gov/ccgg/trends\\_doi.html](https://gml.noaa.gov/ccgg/trends_doi.html) (accessed on 18 March 2022).
8. Jackson, R.B.; Saunio, M.; Bousquet, P.; Canadell, J.G.; Poulter, B.; Stavert, A.R.; Bergamaschi, P.; Niwa, Y.; Segers, A.; Tsuruta, A. Increasing anthropogenic methane emissions arise equally from agricultural and fossil fuel sources. *Environ. Res. Lett.* **2020**, *15*, 071002. [[CrossRef](#)]
9. Höglund-Isaksson, L.; Gómez-Sanabria, A.; Klimont, Z.; Rafaj, P.; Schöpp, W. Technical potentials and costs for reducing global anthropogenic methane emissions in the 2050 timeframe—results from the GAINS model. *Environ. Res. Commun.* **2020**, *2*, 025004. [[CrossRef](#)]
10. Crippa, M.; Dentener, F.; Guizzardi, D.; Janssens-Maenhout, G.; Van Dingenen, R. *Global Trends of Methane Emissions and Their Impacts on Ozone Concentrations*; Publications Office of the European Union: Luxembourg, 2018.
11. Feng, Z.; Kobayashi, K.; Li, P.; Xu, Y.; Tang, H.; Guo, A.; Paoletti, E.; Calatayud, V. Impacts of current ozone pollution on wheat yield in china as estimated with observed ozone, meteorology and day of flowering. *Atmos. Environ.* **2019**, *217*, 116945. [[CrossRef](#)]

12. Avnery, S.; Mauzerall, D.L.; Liu, J.; Horowitz, L.W. Global crop yield reductions due to surface ozone exposure: 1. year 2000 crop production losses and economic damage. *Atmos. Environ.* **2011**, *45*, 2284–2296. [[CrossRef](#)]
13. Mills, G.; Sharps, K.; Simpson, D.; Pleijel, H.; Frei, M.; Burkey, K.; Emberson, L.; Uddling, J.; Broberg, M.; Feng, Z.; et al. Closing the global ozone yield gap: Quantification and cobenefits for multistress tolerance. *Glob. Change Biol.* **2018**, *24*, 4869–4893. [[CrossRef](#)] [[PubMed](#)]
14. Shindell, D.; Smith, C.J. Climate and air-quality benefits of a realistic phase-out of fossil fuels. *Nature* **2019**, *573*, 408–411. [[CrossRef](#)]
15. Bey, I.; Jacob, D.J.; Yantosca, R.M.; Logan, J.A.; Field, B.D.; Fiore, A.M.; Li, Q.; Liu, H.Y.; Mickley, L.J.; Schultz, M.G. Global modeling of tropospheric chemistry with assimilated meteorology: Model description and evaluation. *J. Geophys. Res.* **2001**, *106*, 23073–23095. [[CrossRef](#)]
16. WMO Greenhouse Gas Bulletin. Available online: <https://library.wmo.int/idurl/4/58448> (accessed on 21 August 2022).
17. Van Der Werf, G.R.; Randerson, J.T.; Giglio, L.; Van Leeuwen, T.T.; Chen, Y.; Rogers, B.M.; Mu, M.; Van Marle, M.J.E.; Morton, D.C.; Collatz, G.J.; et al. Global fire emissions estimates during 1997–2016. *Earth Syst. Sci. Data* **2017**, *9*, 697–720. [[CrossRef](#)]
18. Duncan Fairlie, T.; Jacob, D.J.; Park, R.J. The Impact of transpacific transport of mineral dust in the United States. *Atmos. Environ.* **2007**, *41*, 1251–1266. [[CrossRef](#)]
19. Jaeglé, L.; Quinn, P.K.; Bates, T.S.; Alexander, B.; Lin, J.-T. Global distribution of sea salt aerosols: New constraints from in situ and remote sensing observations. *Atmos. Chem. Phys.* **2011**, *11*, 3137–3157. [[CrossRef](#)]
20. Murray, L.T.; Jacob, D.J.; Logan, J.A.; Hudman, R.C.; Koshak, W.J. Optimized regional and interannual variability of lightning in a global chemical transport model constrained by LIS/OTD satellite data. *J. Geophys. Res.* **2012**, *117*, D20307. [[CrossRef](#)]
21. Hudman, R.C.; Moore, N.E.; Mebust, A.K.; Martin, R.V.; Russell, A.R.; Valin, L.C.; Cohen, R.C. Steps towards a mechanistic model of global soil nitric oxide emissions: Implementation and space based-constraints. *Atmos. Chem. Phys.* **2012**, *12*, 7779–7795. [[CrossRef](#)]
22. Guenther, A.B.; Jiang, X.; Heald, C.L.; Sakulyanontvittaya, T.; Duhl, T.; Emmons, L.K.; Wang, X. The Model of Emissions of Gases and Aerosols from Nature Version 2.1 (MEGAN2.1): An extended and updated framework for modeling biogenic emissions. *Geosci. Model Dev.* **2012**, *5*, 1471–1492. [[CrossRef](#)]
23. Rienecker, M.M.; Suarez, M.J.; Gelaro, R.; Todling, R.; Bacmeister, J.; Liu, E.; Bosilovich, M.G.; Schubert, S.D.; Takacs, L.; Kim, G.-K.; et al. MERRA: NASA’s Modern-Era Retrospective Analysis for Research and Applications. *J. Clim.* **2011**, *24*, 3624–3648. [[CrossRef](#)]
24. Molod, A.; Takacs, L.; Suarez, M.; Bacmeister, J. Development of the GEOS-5 atmospheric general circulation model: Evolution from MERRA to MERRA2. *Geosci. Model Dev.* **2014**, *7*, 7575–7611. [[CrossRef](#)]
25. Keller, C.A.; Long, M.S.; Yantosca, R.M.; Da Silva, A.M.; Pawson, S.; Jacob, D.J. HEMCO v1.0: A versatile, ESMF-compliant component for calculating emissions in atmospheric models. *Geosci. Model Dev.* **2014**, *7*, 1409–1417. [[CrossRef](#)]
26. FAO. GAEZ v4 Data Portal. 2021. Available online: <https://gaez.fao.org/pages/data-access-download> (accessed on 11 March 2022).
27. Sacks, W.J.; Deryng, D.; Foley, J.A.; Ramankutty, N. Crop Planting Dates: An analysis of global patterns: Global crop planting dates. *Glob. Ecol. Biogeogr.* **2010**, *19*, 607–620. [[CrossRef](#)]
28. Tai, A.P.K.; Martin, M.V.; Heald, C.L. Threat to future global food security from climate change and ozone air pollution. *Nat. Clim. Change* **2014**, *4*, 817–821. [[CrossRef](#)]
29. Emberson, L.D.; Büker, P.; Ashmore, M.R.; Mills, G.; Jackson, L.S.; Agrawal, M.; Atikuzzaman, M.D.; Cinderby, S.; Engardt, M.; Jamir, C.; et al. A comparison of north american and asian exposure–response data for ozone effects on crop yields. *Atmos. Environ.* **2009**, *43*, 1945–1953. [[CrossRef](#)]
30. Tatsumi, K. Rice yield reductions due to ozone exposure and the roles of VOCs and NO<sub>x</sub> in ozone production in Japan. *J. Agric. Meteorol.* **2022**, *78*, 89–100. [[CrossRef](#)]
31. Wang, X.; Mauzerall, D.L. Characterizing distributions of surface ozone and its impact on grain production in China, Japan and South Korea: 1990 and 2020. *Atmos. Environ.* **2004**, *38*, 4383–4402. [[CrossRef](#)]
32. Schiferl, L.D.; Heald, C.L. Particulate matter air pollution may offset ozone damage to global crop production. *Atmos. Chem. Phys.* **2018**, *18*, 5953–5966. [[CrossRef](#)]
33. Lin, X.; Zhang, W.; Crippa, M.; Peng, S.; Han, P.; Zeng, N.; Yu, L.; Wang, G. A comparative study of anthropogenic CH<sub>4</sub> emissions over China based on the ensembles of bottom-up inventories. *Earth Syst. Sci. Data* **2021**, *13*, 1073–1088. [[CrossRef](#)]
34. Liu, N.; Lin, W.; Ma, J.; Xu, W.; Xu, X. Seasonal variation in surface ozone and its regional characteristics at global atmosphere watch stations in China. *J. Environ. Sci.* **2019**, *77*, 291–302. [[CrossRef](#)]
35. Deb Roy, S.; Beig, G.; Ghude, S.D. Exposure-plant response of ambient ozone over the tropical Indian region. *Atmos. Chem. Phys.* **2009**, *9*, 5253–5260. [[CrossRef](#)]
36. Tai, A.P.K.; Sadiq, M.; Pang, J.Y.S.; Yung, D.H.Y.; Feng, Z. Impacts of surface ozone pollution on global crop yields: Comparing different ozone exposure metrics and incorporating co-effects of CO<sub>2</sub>. *Front. Sustain. Food Syst.* **2021**, *5*, 534616. [[CrossRef](#)]
37. Ghude, S.D.; Jain, S.L.; Arya, B.C.; Beig, G.; Ahammed, Y.N.; Kumar, A.; Tyagi, B. Ozone in ambient air at a tropical megacity, Delhi: Characteristics, trends and cumulative ozone exposure indices. *J. Atmos. Chem.* **2008**, *60*, 237–252. [[CrossRef](#)]
38. Sahu, S.K.; Beig, G.; Sharma, C. Decadal growth of black carbon emissions in India. *Geophys. Res. Lett.* **2008**, *35*, L02807. [[CrossRef](#)]
39. Beig, G.; Ali, K. Behavior of Boundary layer ozone and its precursors over a great alluvial plain of the world: Indo-Gangetic Plains. *Geophys. Res. Lett.* **2006**, *33*, L24813. [[CrossRef](#)]

40. Feng, Z.; Xu, Y.; Kobayashi, K.; Dai, L.; Zhang, T.; Agathokleous, E.; Calatayud, V.; Paoletti, E.; Mukherjee, A.; Agrawal, M.; et al. Ozone pollution threatens the production of major staple crops in East Asia. *Nat. Food* **2022**, *3*, 47–56. [[CrossRef](#)]
41. Wang, P.; Tang, J.; Sun, X.; Wang, S.; Wu, J.; Dong, X.; Fang, J. Heat waves in China: Definitions, leading patterns, and connections to large-scale atmospheric circulation and SSTs. *JGR Atmos.* **2017**, *122*, 10,679–10,699. [[CrossRef](#)]
42. Wang, P.; Yang, Y.; Li, H.; Chen, L.; Dang, R.; Xue, D.; Li, B.; Tang, J.; Leung, L.R.; Liao, H. North China Plain as a hot spot of ozone pollution exacerbated by extreme high temperatures. *Atmos. Chem. Phys.* **2022**, *22*, 4705–4719. [[CrossRef](#)]
43. Li, K.; Jacob, D.J.; Liao, H.; Qiu, Y.; Shen, L.; Zhai, S.; Bates, K.H.; Sulprizio, M.P.; Song, S.; Lu, X.; et al. Ozone pollution in the North China Plain spreading into the late-winter haze season. *Proc. Natl. Acad. Sci. USA* **2021**, *118*, e2015797118. [[CrossRef](#)] [[PubMed](#)]
44. Sharma, A.; Ojha, N.; Pozzer, A.; Beig, G.; Gunthe, S.S. Revisiting the crop yield loss in India attributable to ozone. *Atmos. Environ. X* **2019**, *1*, 100008. [[CrossRef](#)]
45. Ainsworth, E.A. Understanding and improving global crop response to ozone pollution. *Plant J.* **2017**, *90*, 886–897. [[CrossRef](#)] [[PubMed](#)]
46. Wild, O.; Fiore, A.M.; Shindell, D.T.; Doherty, R.M.; Collins, W.J.; Dentener, F.J.; Schultz, M.G.; Gong, S.; MacKenzie, I.A.; Zeng, G.; et al. Modelling future changes in surface ozone: A parameterized approach. *Atmos. Chem. Phys.* **2012**, *12*, 2037–2054. [[CrossRef](#)]
47. Wang, Y.; Jacob, D.J. Anthropogenic forcing on tropospheric ozone and OH since preindustrial times. *J. Geophys. Res.* **1998**, *103*, 31123–31135. [[CrossRef](#)]
48. Parrish, D.D.; Petropavlovskikh, I.; Oltmans, S.J. Reversal of long-term trend in baseline ozone concentrations at the North American West Coast. *Geophys. Res. Lett.* **2017**, *44*, 10675–10681. [[CrossRef](#)]
49. Derwent, R.G.; Manning, A.J.; Simmonds, P.G.; Spain, T.G.; O’Doherty, S. Long-term trends in ozone in baseline and European regionally-polluted air at Mace Head, Ireland over a 30-year period. *Atmos. Environ.* **2018**, *179*, 279–287. [[CrossRef](#)]

**Disclaimer/Publisher’s Note:** The statements, opinions and data contained in all publications are solely those of the individual author(s) and contributor(s) and not of MDPI and/or the editor(s). MDPI and/or the editor(s) disclaim responsibility for any injury to people or property resulting from any ideas, methods, instructions or products referred to in the content.